J. Fluid Mech. (2001), *vol.* 440, *pp.* 1–25. Printed in the United Kingdom

© 2001 Cambridge University Press

Flow about a circular cylinder between parallel walls

By LUIGINO ZOVATTO AND GIANNI PEDRIZZETTI

Dipartimento Ingegneria Civile, Università di Trieste. Piazzale Europa 1, 34127 Trieste, Italy

(Received 6 July 1999 and in revised form 23 January 2001)

The flow about a body placed inside a channel differs from its unbounded counterpart because of the effects of wall confinement, shear in the incoming velocity profile, and separation of vorticity from the channel walls. The case of a circular cylinder placed between two parallel walls is here studied numerically with a finite element method based on the vorticity–streamfunction formulation for values of the Reynolds number consistent with a two-dimensional assumption.

The transition from steady flow to a periodic vortex shedding regime has been analysed: transition is delayed as the body approaches one wall because the interaction between the cylinder wake and the wall boundary layer vorticity constrains the separating shear layer, reducing its oscillations. The results confirm previous observations of the inhibition of vortex shedding for a body placed near one wall. The unsteady vortex shedding regime changes, from a pattern similar to the von Kármán street (with some differences) when the body is in about the centre of the channel, to a single row of same-sign vortices as the body approaches one wall. The separated vortex dynamics leading to this topological modification is presented.

The mean drag coefficients, once they have been normalized properly, are comparable when the cylinder is placed at different distances from one wall, down to gaps less than one cylinder diameter. At smaller gaps the body behaves similarly to a surface-mounted obstacle. The lift force is given by a repulsive component plus an attractive one. The former, well known from literature, is given by the deviation of the wake behind the body. Evidence of the latter, which is a consequence of the shear in front of the body, is given.

1. Introduction

The flow inside a channel in the presence of a circular cylinder is the subject of this work. The channel flow is laminar (Poiseuille) in the absence of the obstacle and the phenomena associated to the presence of the cylinder are studied.

The most relevant feature of the flow, at moderate values of the Reynolds number, e.g. at a Reynolds number (based on the external velocity and cylinder diameter) close to 50, is the instability of the symmetric wake and the onset of a time-periodic regime characterized by alternate vortex shedding, known as the von Kármán vortex street, whose dimensionless period depends on the Reynolds number. By further increasing the Reynolds number a transition to three-dimensional flow occurs around the value 180 (Williamson 1996*a*, *b*; Sohankar, Norberg & Davidson 1999); however the periodic vortex shedding phenomenon remains the large-scale dominant feature even at large Reynolds number in the turbulent wake.

https://doi.org/10.1017/S0022112001004608 Published online by Cambridge University Press

The similarly relevant case of flow about a cylinder in the presence of plane boundaries has received much less attention. The presence of a plane boundary modifies the dynamics, with respect to the unbounded conditions, due to essentially three different factors. (i) The impermeability of the wall gives an irrotational constraint to the cylinder wake which cannot spread without limit. An important effect given by the nearby wall, which is the same as that found in a periodic array of symmetrical pairs of cylinders, is the birth of a finite mean force directed away from the wall (Bearman & Wadcock 1973). (ii) The flow over a rigid wall presents a velocity profile which is not uniform in front of the cylinder. This shear has a non-symmetric influence on the body, and the incoming vorticity profile combines with the vorticity separated from the cylinder. (iii) The presence of a no-slip wall can give rise to a wake-induced boundary layer on the plane boundary. This effect has little influence until the distance from the wall is large, but it eventually modifies the entire wake when the interaction is strong enough to provoke the separation of the boundary layer from the plane wall. In this case a more complex wake structure can develop from the combination of the vorticity shed from the cylinder and from the plane wall.

It should be noted that the phenomena associated with the last two points (ii) and (iii) are not the same when the body is moving in a still fluid or when a stream encounters a fixed body. These two physical conditions, which were the same in unbounded fluid (kinematically the same, while the dynamic actions differ, in unsteady flow, by an analytical term), must be differentiated in the presence of a plane boundary. The interaction of an incoming steady flow over a wall with a cylinder also depends on the height of the boundary layer on the wall. Thus we have an additional external length scale which determines the boundary layer thickness: it can be the upstream length of the plane boundary or, as is the case in this work, the distance to another parallel wall which limits the growth of the boundary layer.

Several experimental results for the flow around a circular cylinder in the presence of a single plane boundary have been reported at moderately high Reynolds number, in a turbulent regime (Bearman & Zdravkovich 1978; Grass *et al.* 1984; Taniguchi & Miyakoshi 1990; Lei, Cheng & Kavanagh 1999). These have shown that the major effects due to the presence of the wall are the modification of the forces on the body as it approaches the wall, a slight variation of the shedding frequency, and the suppression of vortex shedding when the body is closer than a critical distance from the wall. A review of the results for this case is reported in Lei *et al.* (1999). In the presence of one wall Bearman & Zdravkovich (1978) have shown that the wake structure and the shedding rate are about the same as the unbounded case until the cylinder is very close to the surface such that the gap between the body and the wall is as small as 30 to 40% of the body diameter. At smaller distances the wake is almost steady and the periodic shedding is strongly inhibited; in this case they also report a visible separated bubble over the wall. More recent measurements (Lei *et al.* 1999) have shown that the vortex shedding is inhibited when the gap is about 0.2–0.3 diameters, the effective value depending on the thickness of the turbulent boundary layer.

Forces are influenced by the wall along with the modification of the wake; a decrease of the drag coefficient, when normalized with the external flow velocity, is reported by several authors as the body enters the wall boundary layer (Taniguchi & Miyakoshi 1990; Lei *et al.* 1999). The lift force, which is zero far from the wall, is usually directed away from the wall as a consequence of the deviation of the wake behind the body away from the wall and of the reduction of velocity in the gap below the body. However a non-monotonic change in the lift, including in some cases

https://doi.org/10.1017/S0022112001004608 Published online by Cambridge University Press

a change of sign, with the distance from one wall has been observed experimentally (Lei *et al.* 1999). The actual lift in a real flow is evidently also influenced by the presence of an incoming shear; the influence of shear alone has been investigated numerically in laminar flow (Nakabayashi, Yoshida & Aoi 1993) where evidence of an unexplained negative lift is reported.

The case of an oscillatory stream has also received much attention because of its relevance to marine pipelines. The wake structure and related actions on the body in the unbounded domain have been systematically studied in recent years both experimentally and numerically (Tatsuno & Bearman 1990; Justensen 1991; Dütsch *et al.* 1998). The influence of a plane boundary in the oscillatory regime was studied experimentally (Sumer, Jensen & Fredsoe 1991) in the case of cylinder moving in a still fluid. As in the steady case, a mean lift force away from the wall is experienced by the body as it approaches it. The shedding regimes are influenced by the presence of the wall at distances comparable with the cylinder diameter. However it must be remembered that the separated vortex fields in the case of oscillatory flow are more complex than in steady flow and a more marked influence of the wall should be expected. When the distance is small enough the vortex shedding is almost completely suppressed because of the interaction with the wall boundary layer separation.

The present work is focused on the interaction between a laminar stream in a plane channel and a small circular cylinder placed inside it. The undisturbed velocity profile is parabolic and the dynamics about the cylinder are studied, varying the Reynolds number, as a function of the cylinder position inside the channel. It is evident from the results cited above that the influence of the wall is felt only when the body is at a distance comparable with or smaller than its diameter; therefore as the body approaches one wall, the influence of the other channel wall is limited to a confinement of the flow, or blockage effect, and this study also describes shear flow over a cylinder near a plane boundary. This study has been stimulated by the need to predict the spurious effects associated with the insertion of probes or wires in a conduit in the laminar regime. However it has other applications; for example, the presence of wake vorticity enhances transport and mixing, and it has been shown that heat transport in a laminar channel flow in the presence of a row of cylinders can reach levels comparable with those of turbulent channel flow with a smaller energy dissipation (Karniadakis, Mikic & Patera 1988).

The flow past a cylinder in a channel flow has been studied for the cylinder placed symmetrically in the centre of the channel (Chen, Pritchard & Tavener 1995). That study focused on the nature and occurrence of the bifurcation from steady symmetric flow to the periodic shedding regime. In that case the channel walls were introduced as a possible means of eliminating the discrepancies found experimentally and numerically for the bifurcation Reynolds number in an unbounded domain, which are assumed to be due to different approximations of the unboundness idealization. That study was performed numerically with a finite element method in primitive variables; an eigenvalue calculation was also presented to better localize the critical value of the parameters. In the confined flow, which is easier to reproduce, the bifurcation was found to be of Hopf type; these results are compared with ours in the case of a symmetrically placed cylinder. The case of a body between frictionless walls (symmetry condition) has been considered (see for example Sohankar *et al.* 1999): the walls simply give the (irrotational) local acceleration effect due to the blocking by the body.

In the present study the two-dimensional Navier–Stokes equations are solved in the non-regular domain by a finite element method with a vorticity–streamfunction formu-

https://doi.org/10.1017/S0022112001004608 Published online by Cambridge University Press

lation such that the continuity equation is satisfied exactly. Any three-dimensional effect is therefore neglected and the results are pertinent only for values of the Reynolds number low enough to guarantee the stability of the flow to three-dimensional disturbances. In the absence of specific results regarding the stability to three-dimensional disturbances of a channel flow with an immersed body, the reliability of the two-dimensional assumption depends on (*a*) the stability of a plane channel flow, and (*b*) the stability of the flow about a cylinder in unbounded flow; and (*c*) whether the combined dynamics would be expected to enhance or reduce the stability of the flow.

Linear theory for channel flow predicts that two-dimensional disturbances are unstable at a lower Reynolds number than three-dimensional ones; in fact these are the first to grow, even though they are in turn unstable to three-dimensional perturbations, and are found to become unstable for values of the channel-based Reynolds number above 3000. The transition from two-dimensional to three-dimensional flow in the wake of a circular cylinder has been analysed through a number of experimental results (Williamson 1996*b*), and also reviewed in Williamson (1996*a*). The transition is due to an instability of the rectilinear wake-vortex filament pairs: a waviness of the filaments produces a mutual streamwise stretching resulting in a tendency for it to grow; when the Reynolds number is large enough that the growth rate dominates over the viscous damping rate the wake becomes unstable and eventually it gives rise to vortex loops and streamwise vorticity. Such a transition occurs at a cylinder-based Reynolds number above approximately 180 (in ideal conditions the critical value is about 194, Williamson 1996*a*). The present study is limited to values of the cylinder-based Reynolds number below these limits, and the only simulations produced outside this range, in the extreme case of the body very close to one channel wall, are just for the sake of completing a two-parameters domain picture. It is mentioned above that experiments (Bearman & Zdravkovich 1978; Grass *et al.* 1984; Taniguchi & Miyakoshi 1990; Lei *et al.* 1999) in the turbulent regime indicate that, as the body approaches one wall, the flow possibly suppresses unsteady vortex shedding, or the wake becomes a single row of vortex filaments, rather than pairs, for which the three-dimensional instability found in unbounded flow does not apply. These results, together with the ones found here, suggest, although there is no proof, enhanced stability properties and that the transition to three-dimensional flow may more likely be delayed by the presence of nearby walls.

This work aims to address questions regarding the characteristics of the vortex shedding regime and its modifications, either qualitatively and quantitatively, as the body approaches one wall as Reynolds number varies in the range from the transition to the periodic shedding regime to values where the two-dimensional approximation is physically representative. The features of the separated vorticity dynamics are analysed at different conditions with particular attention to the interaction between the cylinder wake and the induced separation on the plane walls. The presence of the plane boundaries modifies the shedding frequencies and their dependence on the Reynolds number. The value of the critical Reynolds number is shown to vary with the distance from the boundary; the suppression of vortex shedding, observed experimentally in different conditions (Bearman & Zdravkovich 1978; Sumer *et al.* 1991; Lei *et al.* 1999), is also verified, and the influence of the walls on the forces acting on the body is analysed and compared with previous findings.

The mathematical problem is formulated in § 2 and the numerical method is described in § 3. Numerical results for the flow characteristics are presented and discussed in § 4, and for the phenomena related to the forces acting on the body in § 5. A concluding discussion and a summary of results is presented in § 6.

https://doi.org/10.1017/S0022112001004608 Published online by Cambridge University Press

2. Mathematical formulation

A plane channel with rectilinear walls separated by a distance H, contains a circular cylinder of diameter D, whose position is defined by the gap Δ, the minimal distance from the cylinder surface to the nearest wall. Consider an incompressible fluid, with density ρ and kinematic viscosity ν, flowing with steady average velocity U inside the channel. The problem can be made dimensionless by taking H as the unit length, H/U as the unit time, and ρH^3 as the unit mass. The problem is governed by three dimensionless parameters: the channel Reynolds number $Re = UH/\nu$, the blockage ratio $d = D/H$, and the gap parameter $\gamma = \Delta/D$. The gap is a positive number which, for symmetry reasons, takes its maximum value $\gamma = (1-d)/2d$ when the cylinder is placed in the centre of the channel.

We are interested in the case of a relatively small cylinder, so that a fixed value $d = 0.2$ of the blockage ratio is assumed throughout this study. The influence on the blockage ratio has been investigated by Chen *et al.* (1995) for the case of a centred cylinder where it is shown that no qualitative change occurs in the flow for blockage ratio below 0.5. In the limiting case, when $d \ll 1$, the flow is essentially independent of the blockage ratio. The dependence on the Reynolds number Re and on the gap γ, now confined to the range $0 \leqslant \gamma \leqslant 2$, is studied here.

Assume a Cartesian system of coordinates $\{x, y\}$ with the x-axis along the centreline of the channel. The governing equations are the plane Navier–Stokes equations which are written in the vorticity–streamfunction formulation:

$$\frac{\partial \omega}{\partial t} + \frac{\partial \psi}{\partial y}\frac{\partial \omega}{\partial x} - \frac{\partial \psi}{\partial x}\frac{\partial \omega}{\partial y} = \frac{1}{Re}\left(\frac{\partial^2 \omega}{\partial x^2} + \frac{\partial^2 \omega}{\partial y^2}\right), \tag{1}$$

where $\omega(x, y, t)$ is the vorticity and $\psi(x, y, t)$ is the streamfunction. Vorticity and streamfunction are related by the Poisson equation

$$\frac{\partial^2 \psi}{\partial x^2} + \frac{\partial^2 \psi}{\partial y^2} = -\omega; \tag{2}$$

in this formulation the continuity equation is automatically satisfied, and the divergence-free velocity field can be computed from the streamfunction (Batchelor 1967).

Equations (1) and (2) must be completed with the boundary conditions. Infinitely upstream and downstream the flow is assumed to be independent of x. On the rigid walls, channel walls and cylinder surface, the velocity vector must vanish and thus the tangential and the normal derivatives of the streamfunction are zero. At the lower and upper channel walls the constant streamfunction values can be obtained *a priori* by the value of the mean velocity to give $\psi = 0$ and $\psi = 1$ respectively. The conditions on the streamfunction are used in the numerical method to express the vorticity at the walls.

3. Numerical method

The space domain is discretized with triangular finite elements. For maximum simplicity, the variables have been assumed to change linearly within every element. Differential equations (1) and (2) are rewritten on the finite element mesh using a Galerkin residual procedure (Zienkiewicz 1977), resulting in a second-order accuracy in space.

https://doi.org/10.1017/S0022112001004608 Published online by Cambridge University Press

The vorticity equation can be written in matrix form as

$$\mathbb{B}\frac{\mathrm{d}\omega}{\mathrm{d}t} + \mathbb{C}(\psi)\,\omega + \frac{1}{Re}\mathbb{K}\,\omega = 0, \tag{3}$$

where ω and ψ now represent the vector of the values of vorticity and streamfunction at the nodes of each element; $\mathbb{B}$ is the element mass matrix, $\mathbb{K}$ is the stiffness matrix which corresponds to the discretized Laplace operator, and $\mathbb{C}(\psi)$ represents the nonlinear operator applied to vorticity. The Poisson equation, discretized as

$$\mathbb{K}\psi = \mathbb{B}\omega, \tag{4}$$

allows us to determine the value of ψ once the vorticity is known at all points internal to the domain.

Equation (3) is discretized in time with a second-order scheme fully implicit for the viscous term; the vorticity field is thus advanced in time by solving

$$\mathbb{B}\frac{(3\omega^{(n+1)} - 4\omega^{(n)} + \omega^{(n-1)})}{2\Delta t} + \mathbb{C}(\psi^{(*)})\omega^{(*)} + \frac{1}{Re}\mathbb{K}\omega^{(n+1)} = 0, \tag{5}$$

where the superscript $^{(n)}$ represents the nth time step, while the superscript $^{(*)}$ corresponds to the extrapolation $f^{(*)} = 2f^{(n)} - f^{(n-1)}$.

Boundary conditions are given at the inlet by prescribing the Poiseuille profile; this gives a Dirichlet condition for either the vorticity or the streamfunction. At the outlet, far downstream, the Neumann condition of zero normal derivative is imposed. At the upper and lower walls the value of the streamfunction is imposed directly; on the cylinder wall the constancy of the streamfunction (to an unknown value) is imposed by a local modification to the stiffness matrix in equation (4). In this way the Poisson equation is not satisfied at the walls because it is substituted by the streamfunction boundary conditions. The value of vorticity at the rigid walls is computed by back-solving equation (4) with unknowns the values of ω at the walls; the no-slip condition of zero normal derivative for the streamfunction is automatically satisfied by elimination of the 'flux of streamfunction' in the residual Galerkin formulation (Saìac, Santi & Mai 1995). This procedure gives the same order of accuracy for the calculation of the vorticity at the wall and at the internal points.

The numerical results were obtained by the solution of the equation over meshes of finite elements. The infinite-length domain was reduced to a finite domain contained between $x = -3$ and $x = +8$; at this downstream end, which corresponds to 40 cylinder diameters, a flow constant along x was well established. A few trials were performed with a longer numerical domain extended up to $x = 10$ with no appreciable differences in the results either in the steady or unsteady cases.

The number of nodes employed for the discretization ranges from 5438 nodes (10 509 elements), for the symmetric, $\gamma = 2$, case, to 9267 nodes (17 728 elements) for the $\gamma = 0.25$ case. The same mesh was used, at a given γ, for all Reynolds numbers, which means that some lower Reynolds number simulations could be performed with a smaller number of nodes. Care was used in refining the grid around the cylinder, downstream of it, and near the walls, so that the typical size of smaller elements is about 5×10^{-3}. The timestep was chosen to satisfy the convective stability condition and the diffusive accuracy, and generally a maximum value of $\Delta t = 5 \times 10^{-3}$ was used.

A grid refinement test was performed for the $\gamma = 2$ and $\gamma = 0.75$ cases at $Re = 500, 1000$. The grid was refined by dividing each triangular element into four smaller ones; in this way the typical grid size is halved. One snapshot of the instantaneous

https://doi.org/10.1017/S0022112001004608 Published online by Cambridge University Press

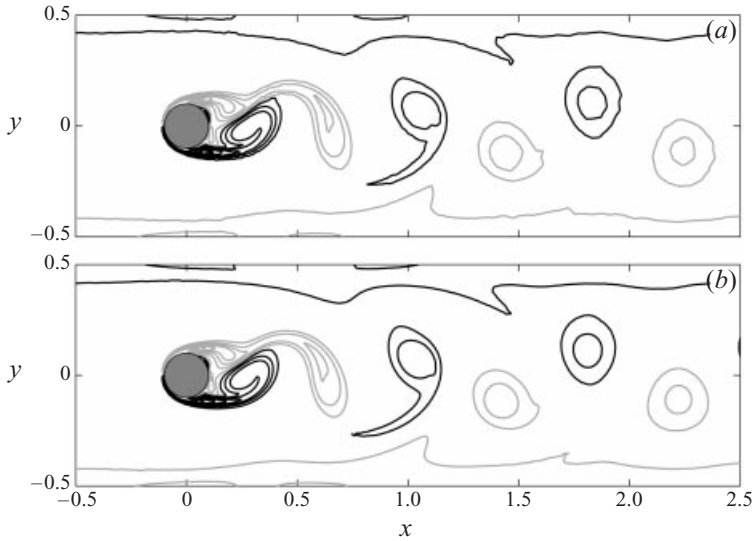


FIGURE 1. Instantaneous flow vorticity contours for $Re = 1000$ and $\gamma = 2$: (*a*) normal grid, (*b*) refined grid. Here and in similar following figures, contour levels increase/decrease from ± 5 in steps of ± 10; positive levels (black lines), negative (grey).

vorticity field is plotted in figure 1(*a*), at $\gamma = 2$, $Re = 1000$, for the grid normally used and in 1(*b*) for the refined one. Smoother contours can be seen in the refined calculation, in particular at low vorticity levels; however no significant physical difference can be detected. Note that the contour lines reported here, and throughout the paper, are drawn directly as straight lines across each (linear) element without any artificial smoothing applied to the curve as a whole.

Every simulation was impulsively started from the irrotational field, and in all cases the steady or periodic regimes are reached after about 20 to 30 time units.

4. Flow features and transition

4.1. *Transition*

Let us first consider the case when the cylinder is placed in the centre of the channel, i.e. $\gamma = 2$. This case has been previously studied by Chen *et al.* (1995) where it has been shown that the flow is steady when the Reynolds number is below a critical value, $Re = 231$, and a periodic shedding regime occurs for larger values of the Reynolds number. This behaviour is analogous to what happens in an unbounded field where the critical value of the cylinder-based Reynolds number is approximately 50. A cylinder-based Reynolds number can be constructed for the present case as

$$Re_{cyl} = Re\, v_{cyl}\, d, \tag{6}$$

where v_{cyl} is the average velocity in front of the cylinder far upstream

$$v_{cyl}(\gamma) = \frac{1}{d}\int_{\gamma d-(1/2)}^{\gamma d+d-(1/2)} v_x(y)\,\mathrm{d}y = -6d^2\gamma^2 + 6d(1-d)\gamma + d(3-2d), \tag{7}$$

and $v_x(y) = 6(1/4 - y^2)$ is the upstream Poiseuille velocity profile. The critical value, corresponding to $Re = 231$, of this cylinder-based Reynolds number $Re_{cyl} \simeq 68$ is slightly larger than in the unbounded case; the local acceleration, caused by the

https://doi.org/10.1017/S0022112001004608 Published online by Cambridge University Press

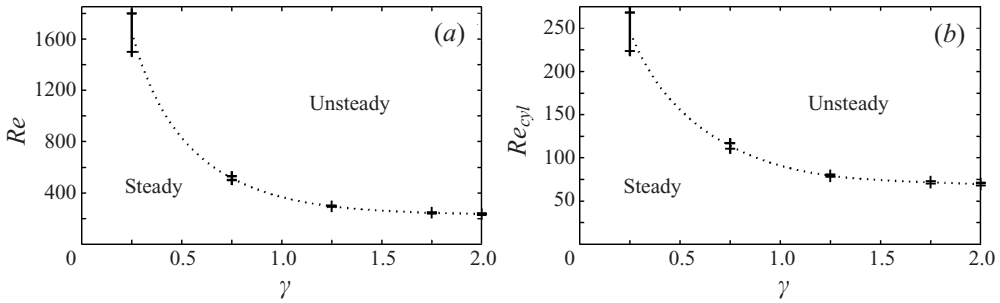


FIGURE 2. Critical (*a*) Reynolds number and (*b*) cylinder-based Reynolds number as a function of the gap parameter.

wall confinement and by the blockage, presumably stabilizes the flow and delays the occurrence of instability (Sohankar *et al.* 1999).

The transition from steady flow to the time-periodic regime is further delayed when the cylinder approaches one wall. The dependence of the critical Reynolds number on the gap parameter is shown in figure 2(*a*). When the cylinder is placed symmetrically between the walls, $\gamma = 2$, we have numerically confirmed that the transition is between $Re = 230$ and $Re = 240$. As the gap is reduced there is a rapid increase in the value of the critical Reynolds number and eventually the transition occurs between $Re = 1500$ and $Re = 1800$ when the gap is reduced to $\gamma = 0.25$. This delay of the transition might first be thought to be attributable to the velocity profile, that is to the reduction of the velocity in front of the body as it approaches one wall which corresponds to a reduction of the local Reynolds number Re_{cyl}. To show that this is not sufficient to explain the transition delay, the dependence of the critical value of the cylinder-based Reynolds number with the gap parameter is plotted in figure 2(*b*). The shape of the two curves in figure 2 is essentially the same.

The different local velocity does not explain the increase of the critical Reynolds number as the cylinder approaches one wall. Neither can an explanation be found in the local irrotational acceleration which occurs only on one side of the body and is reduced on the opposite side. As the body approaches one wall a local acceleration and deceleration occurs on the wall itself; this produces higher vorticity values in the wall boundary layer corresponding to the body, and the boundary layer then rapidly grows downstream and influences the cylinder wake on the side facing the wall. The cylinder wake on the wall side is stabilized by the coupling with the wall vorticity, and so it does not oscillate easily in a shedding regime as it is shown below. This phenomenon is increasingly relevant as the body approaches the wall as can be seen in figure 2 as $\gamma < 1$.

4.2. *Flow features*

The flow in the steady-state regimes is reported in figure 3, at $Re = 200$, for five different values of the gap parameter. The positive (black lines) and negative (grey) vorticity isolines are shown from values ± 5 with a constant increase of ± 10 units for all the pictures (and following similar figures). When the cylinder is placed in the centre of the channel the wake is symmetric and resembles the unbounded case. As the cylinder approaches one wall the wake vorticity on the wall side is significantly reduced in length. On the opposite face of the cylinder the wake elongates, smooths out and eventually combines with the oncoming vorticity of the Poiseuille profile. Decreasing the gap value, it can be seen that the wall-side wake couples with the

https://doi.org/10.1017/S0022112001004608 Published online by Cambridge University Press

wall boundary-layer vorticity of opposite sign while the actual wake is dominated by the vorticity shed from other side of the body; when $\gamma = 0.25$ the wall-side wake has almost disappeared and the wake flow resembles that of a surface-mounted obstacle. The coupling between cylinder and wall vorticity can explain the observed quasi-suppression of shedding found experimentally for $\gamma < 0.3$ in a turbulent boundary layer (Bearman & Zdravkovich 1978; Taniguchi & Miyakoshi 1990; Lei *et al.* 1999) and in an oscillating flow (Sumer *et al.* 1991).

The unsteady periodic shedding regime is shown in figure 4(*a–d*) for an almost symmetric geometry, $\gamma = 1.75$, for $Re = 1000$. The dimensionless shedding period for this case is $T = 0.68$ and instantaneous vorticity fields are shown in figure 4(*a–d*) at time intervals $\Delta t = 0.2$. The time-averaged vorticity field over one period is shown in figure 4(*e*). In this case the wake has already lost the symmetry and a weak dominance of the vorticity shed from the side farther from the wall (clockwise, negative vorticity) is noticeable. However the structure is analogous to the classic von Kármán vortex street with a remarkable difference given by the wall confinement: the trajectories of shed vortices cross each other and the final vertical position is opposite with respect to the unbounded case. Clockwise vortices, separated from the upper side of the cylinder, occupy the lower position in the street while counterclockwise vortices occupy the upper side of the street (see also figure 1). This phenomenon, due to the walls that repel the forming wake, represents a weak kind of interaction in the sense that the cylinder wake is unable to produce any boundary layer separation on the wall.

The case of the cylinder closer to one wall is reported in figure 5 for the same Reynolds number and $\gamma = 1.25$ which corresponds to a period $T = 0.71$. Instantaneous vorticity fields are shown in figure 5(*a–d*) every $\Delta t = 0.2$; the period-averaged vorticity is plotted in figure 5(*e*). The lack of symmetry is evident at this distance. The street of vortices is composed of well-defined negative vortices shed from the upper side of the cylinder and weaker positive ones shed from below. In fact the positive vorticity shed from the wall side of the cylinder begins to interact with the boundary-layer negative vorticity of the plane wall. The shed vorticity is stretched during the pairing with the opposite-sign vorticity, which delays the roll-up into a well-defined vortex and reduces the circulation of the eventual wake vortex because of the dissipative nature of the stretching process. The period-averaged vorticity shows a wake which is deflected away from the wall even though the front stagnation point remained essentially centred; the period-averaged boundary layer at the lower wall presents a maximum of wall vorticity corresponding to the body which falls to a minimum after it. The interaction of the body with the nearby wall is shown in figure 6 where the time-evolution of the positive and negative wall shear stress regions are reported corresponding to the fields of figure 5; an enlarged view of figure 5(*d*) is shown in the background for clarity. This space–time representation allows the evolution of separation and reattachment points to be followed and indicates the unsteady features of the interacting separations (Pedrizzetti 1996). The vorticity separated from the lower side of the cylinder and the flow acceleration create growth of the vorticity in the facing wall boundary layer; this boundary layer is slightly decelerated after the contraction due to the cylinder and is decelerated further by the clockwise vortex separated from the upper side of the body. Such a deceleration is enough to produce weak secondary vorticity on the wall (shown darker grey in the picture) and an unsteady boundary-layer separation from the wall. The separated vorticity then interacts with the lower-wall wake vortex reducing its strength.

When the cylinder approaches closer to the wall the interaction between cylinder

https://doi.org/10.1017/S0022112001004608 Published online by Cambridge University Press

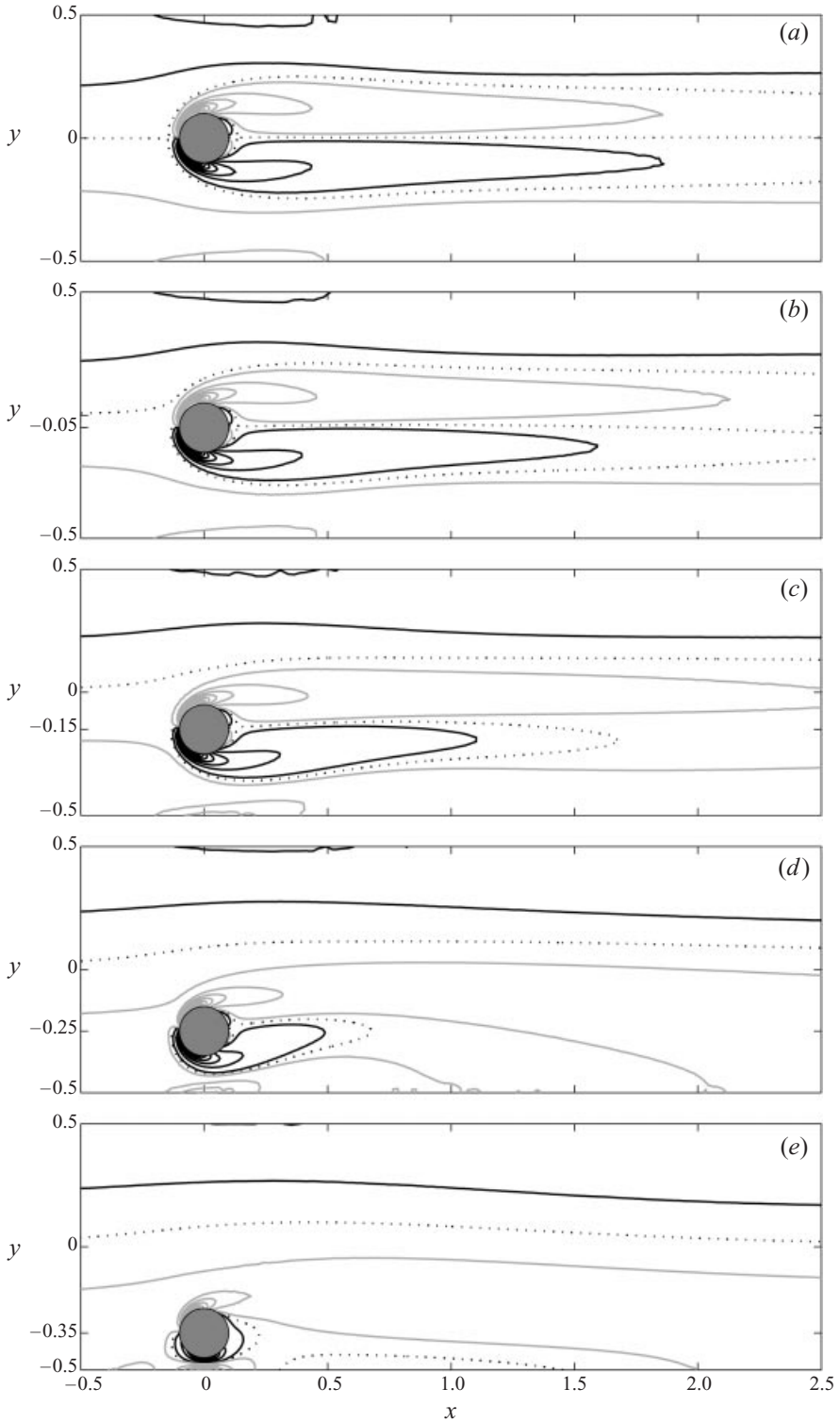


FIGURE 3. Steady flow vorticity contours for $Re = 200$, and (*a*) $\gamma = 2$, (*b*) $\gamma = 1.75$, (*c*) $\gamma = 1.25$, (*d*) $\gamma = 0.75$, (*e*) $\gamma = 0.25$.

https://doi.org/10.1017/S0022112001004608 Published online by Cambridge University Press

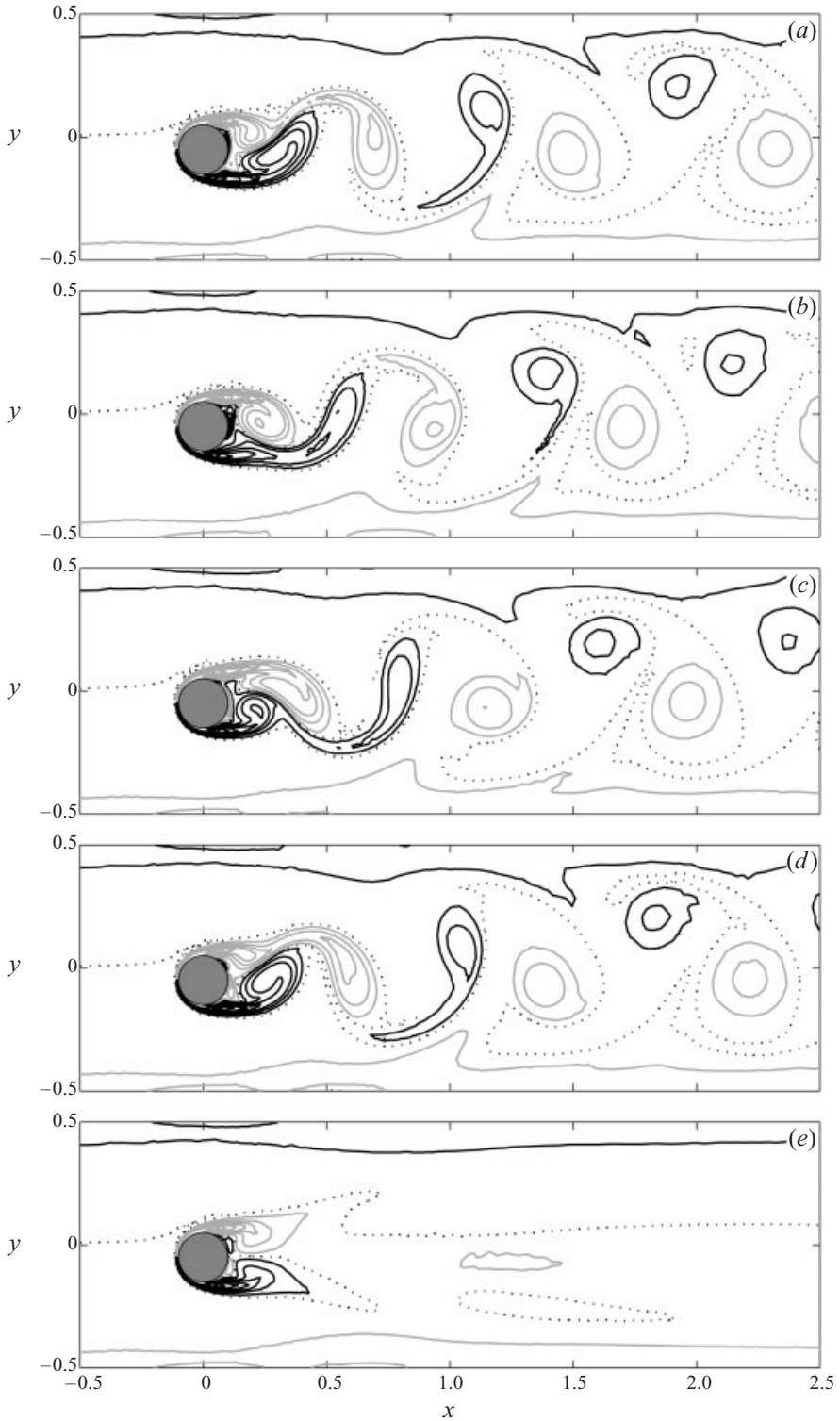


FIGURE 4. Unsteady flow vorticity contours for $Re = 1000$ and $\gamma = 1.75$: (*a–d*) instantaneous vorticity during one period ($T = 0.68$) with time increasing from *a* to *d* in steps of 0.2 time units; (*e*) period-averaged vorticity.

https://doi.org/10.1017/S0022112001004608 Published online by Cambridge University Press

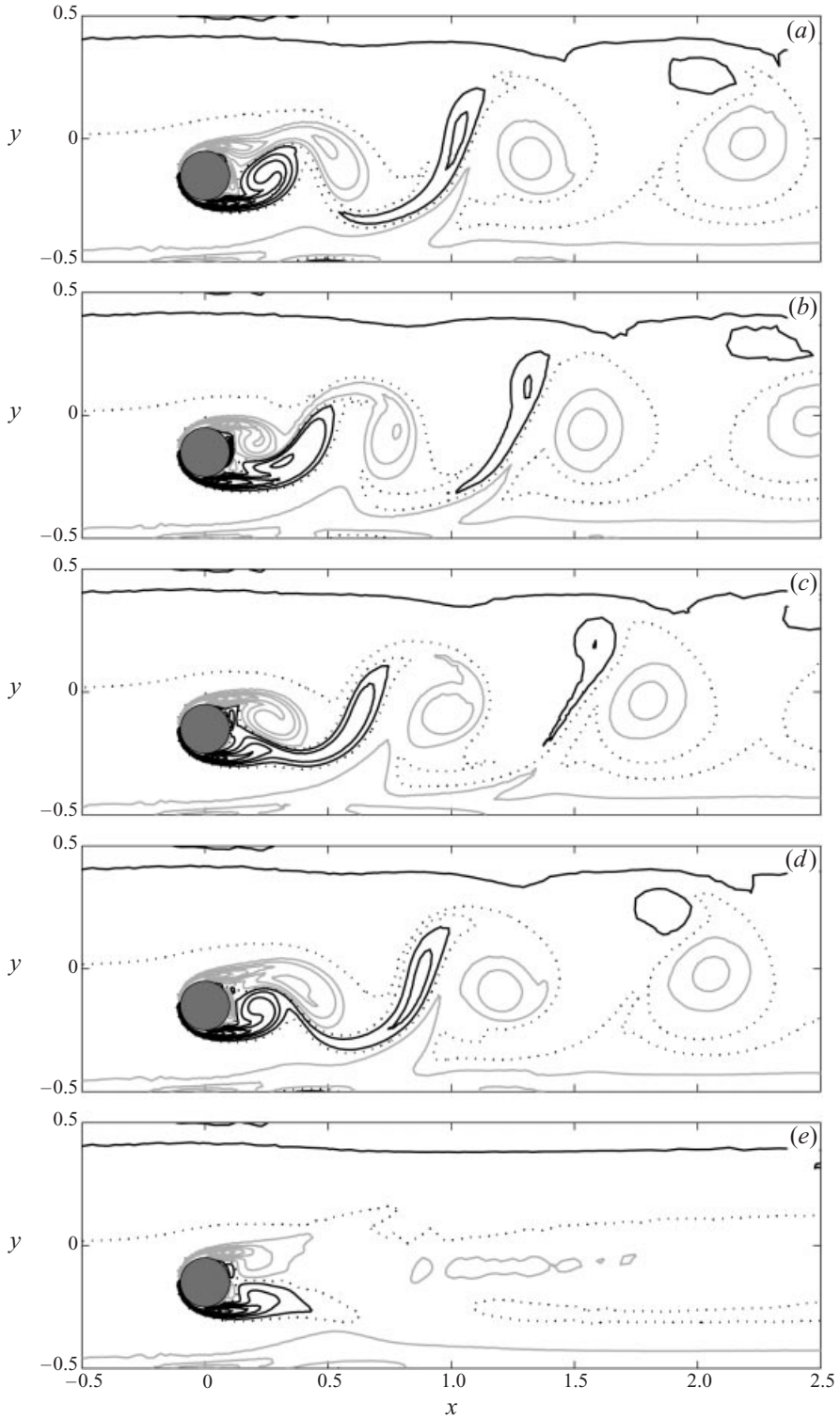


FIGURE 5. Unsteady flow vorticity contours for $Re = 1000$ and $\gamma = 1.25$: (*a–d*) instantaneous vorticity during one period ($T = 0.71$) with time increasing from *a* to *d* in steps of 0.2 time units; (*e*) period-averaged vorticity.

https://doi.org/10.1017/S0022112001004608 Published online by Cambridge University Press

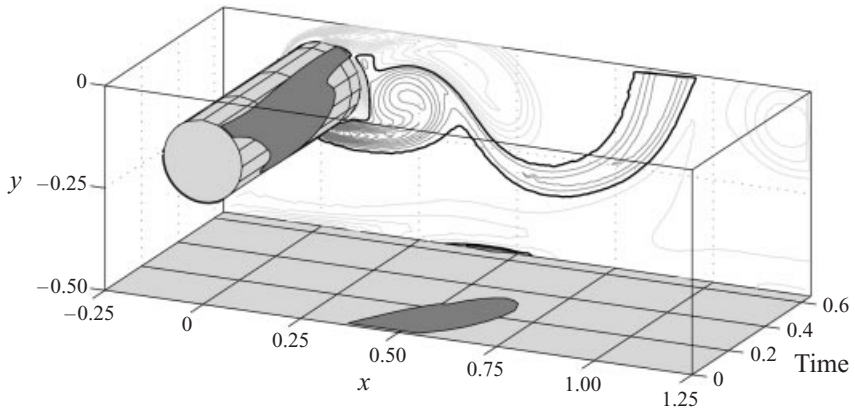


FIGURE 6. Space–time development of wall shear stress during one period for $Re = 1000$ and $\gamma = 1.25$; negative (clockwise wall vorticity) is shown darker grey. Background: instantaneous vorticity field contours, corresponding to figure 5(*d*), at levels from 0 in steps of ± 5; positive levels (darker grey), negative (light grey), zero (black).

wake and wall vorticity is more marked. This is shown in figure 7 at the same Reynolds number and $\gamma = 0.75$ whose corresponding period is $T = 0.78$. Instantaneous vorticity fields are shown in figure 7(*a–d*) every $\Delta t = 0.2$; the period-averaged vorticity is plotted in figure 7(*e*). At this distance the wall side of the cylinder is unable to shed any vortices and the final wake is composed of a single row of same-sign vortices shed from the opposite side. The vorticity separating from the cylinder on the side facing the wall begins to roll-up but is rapidly stretched by the wall vorticity of opposite sign. Thus part of it remains attached to the cylinder to form a quasi-steady attached wake, while the farther part does not roll up and forms, with the wall vorticity, a pair of opposite-sign vortex sheets which are dissipated during the mutual stretching process. As a result the major oscillations of the periodic shedding dynamics are found farther downstream of the cylinder rather than on the body itself. The steady vorticity has a three-layer structure, which is slightly deflected away from the wall, where the wall vorticity is coupled with the wake on the cylinder's wall side. The regularity of the row of single vortices is shown by the appearance of the period-average single-signed elongated shear layer few diameters downstream the body.

The wall shear stress space–time evolution is reported in figure 8 for the same parameters ($Re = 1000$, $\gamma = 0.75$). The reattachment point at the rear of the cylinder has a significantly reduced oscillation indicating that the separating shear layer on the lower side of the body is constrained by the presence of the closer wall. The vorticity boundary layer which is created at the wall below the body is subjected to a deceleration after the body which is also due to the vicinity of the same-sign vortex separated from the upper side of the cylinder. The boundary layer vorticity separates from the wall and is dissipated during its pairing with the nearby wake vorticity; nevertheless a wall layer of secondary vorticity is maintained, induced by the single vortex wake.

When the cylinder is even closer to one wall, it approaches the case of a surface-mounted obstacle with one recirculating bubble downstream which becomes unstable at large Reynolds number. (Note however that at such large *Re* the two-dimensional flow may become unstable to three-dimensional disturbances and the plane approximation is no longer physically representative.)

The shedding frequencies have been evaluated from signals of several flow quantities

https://doi.org/10.1017/S0022112001004608 Published online by Cambridge University Press

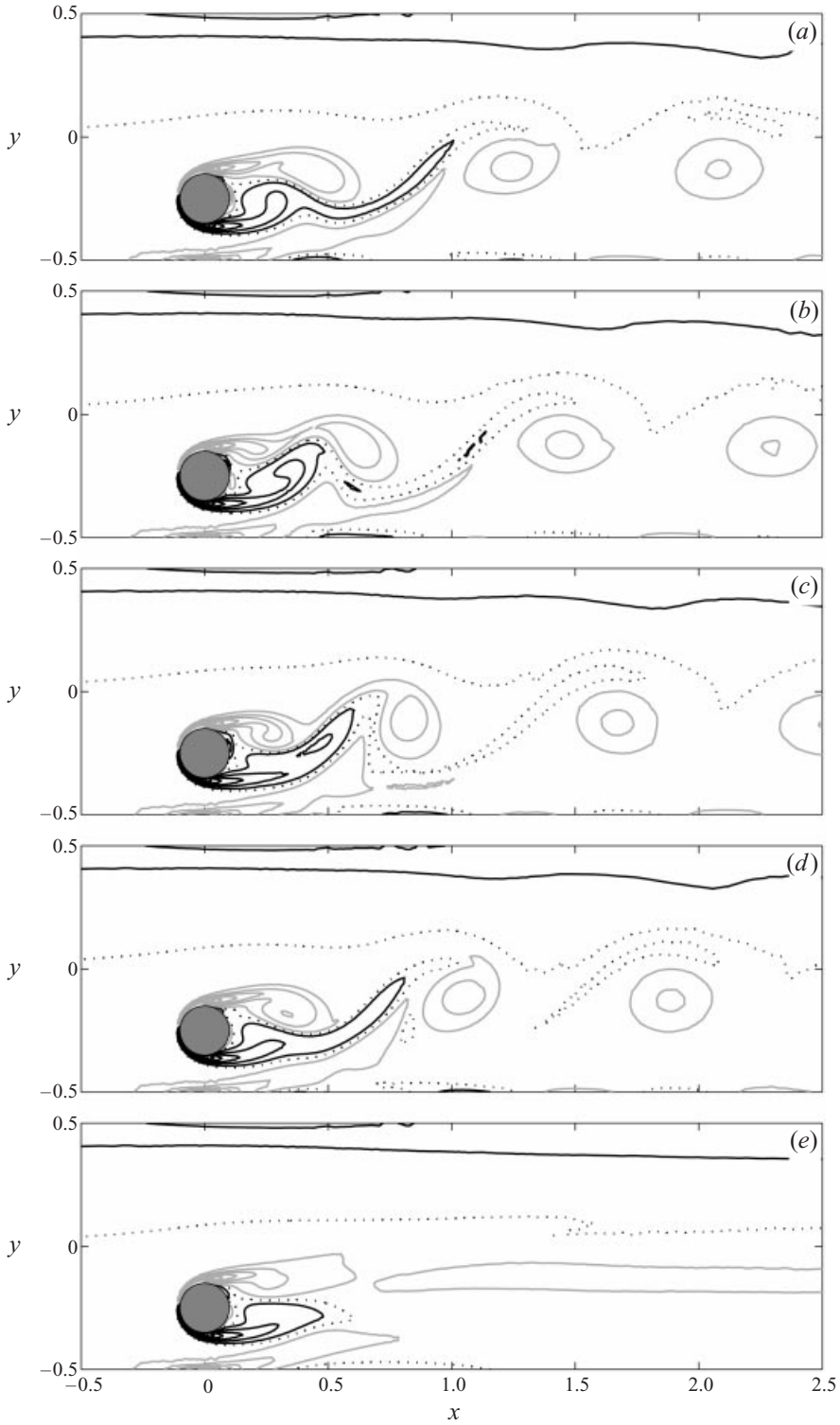


FIGURE 7. Unsteady flow vorticity contours for $Re = 1000$ and $\gamma = 0.75$; (*a–d*) instantaneous vorticity during one period ($T = 0.78$) with time increasing from *a* to *d* in steps of 0.2 time units; (*e*) period-averaged vorticity.

https://doi.org/10.1017/S0022112001004608 Published online by Cambridge University Press

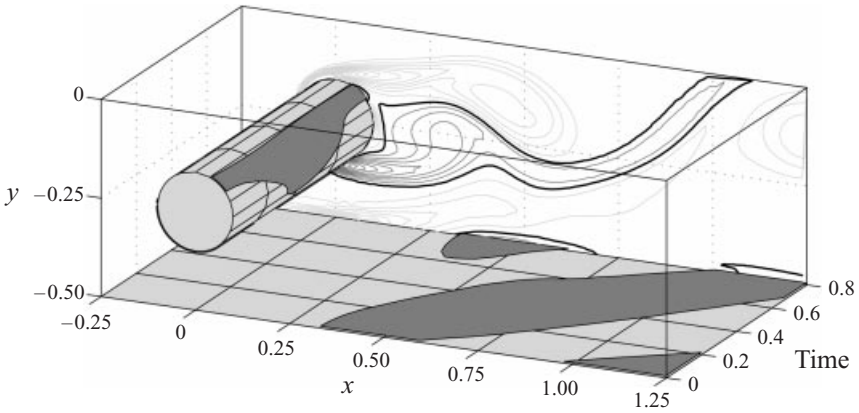


FIGURE 8. Space–time development of wall shear stress during one period for $Re = 1000$ and $\gamma = 0.75$; negative (clockwise wall vorticity) is shown darker grey. Background: instantaneous vorticity field contours at levels from 0 in steps of ± 5; positive levels (darker grey), negative (light grey), zero (black).

(vorticity at different points, forces) and the time signals were always essentially sinusoidal. Their spectra revealed some energy at frequencies that are multiples of the fundamental one only at the higher Reynolds values, although the secondary peak was at most 3 orders of magnitude smaller than the fundamental one. The dimensionless period of the periodic regimes is reported in table 1 as a function of the Reynolds number and the gap parameter. The result for the symmetric case is in general agreement with the unbounded case when the latter is compared with the cylinder-based Strouhal number $d/v_{cyl}T$. This ranges approximately from 0.16 for $Re_{cyl} = 70$ to 0.2 for $Re_{cyl} = 1000$. The Reynolds number dependence is analogous when the cylinder is at a smaller distance from one wall, with differences given by the different values of the critical Reynolds number (the case $\gamma = 0.75$, $Re = 500$ is shown in parentheses because the weak oscillation is decaying extremely slowly and we cannot guarantee if it will eventually disappear or settle to a very small but non-zero value). Notice that, for all values of the gap parameter, the period at the onset of the unsteady regime is approximately the same. The approach to one wall, when the Reynolds number is sufficiently high to have a well-developed von Kármán flow, gives an increase of the period and eventually inhibits the unsteady shedding regime.

The effect of a variation in the Reynolds number is shown in figure 9(*a–e*) where the isovorticity lines are plotted, for $\gamma = 0.75$, at $Re = 100, 200, 300, 500, 700$ (*a* to *e*, respectively; pictures a, b, c represent steady fields whereas pictures d, e are instantaneous snapshots during the periodic regime; the corresponding case at $Re = 1000$ can be seen in figure 7). As expected an increase in the Reynolds number corresponds to a more persistent wake which elongates farther downstream. When the wake is long enough it begins to fluctuate at the downstream tail; at increasing Re the oscillation influences a larger portion of the wake. This mechanism looks to be the same as the unbounded case despite the apparent physical difference, in particular the fact that transition is here not related to an evident symmetry breaking.

5. Forces

The forces acting on the cylinder have been calculated by integration of the wall pressure and wall shear stress on the cylinder surface. The presence of the wall influences the pressure distribution on the body (Bearman & Zdravkovich 1978; Lei

https://doi.org/10.1017/S0022112001004608 Published online by Cambridge University Press

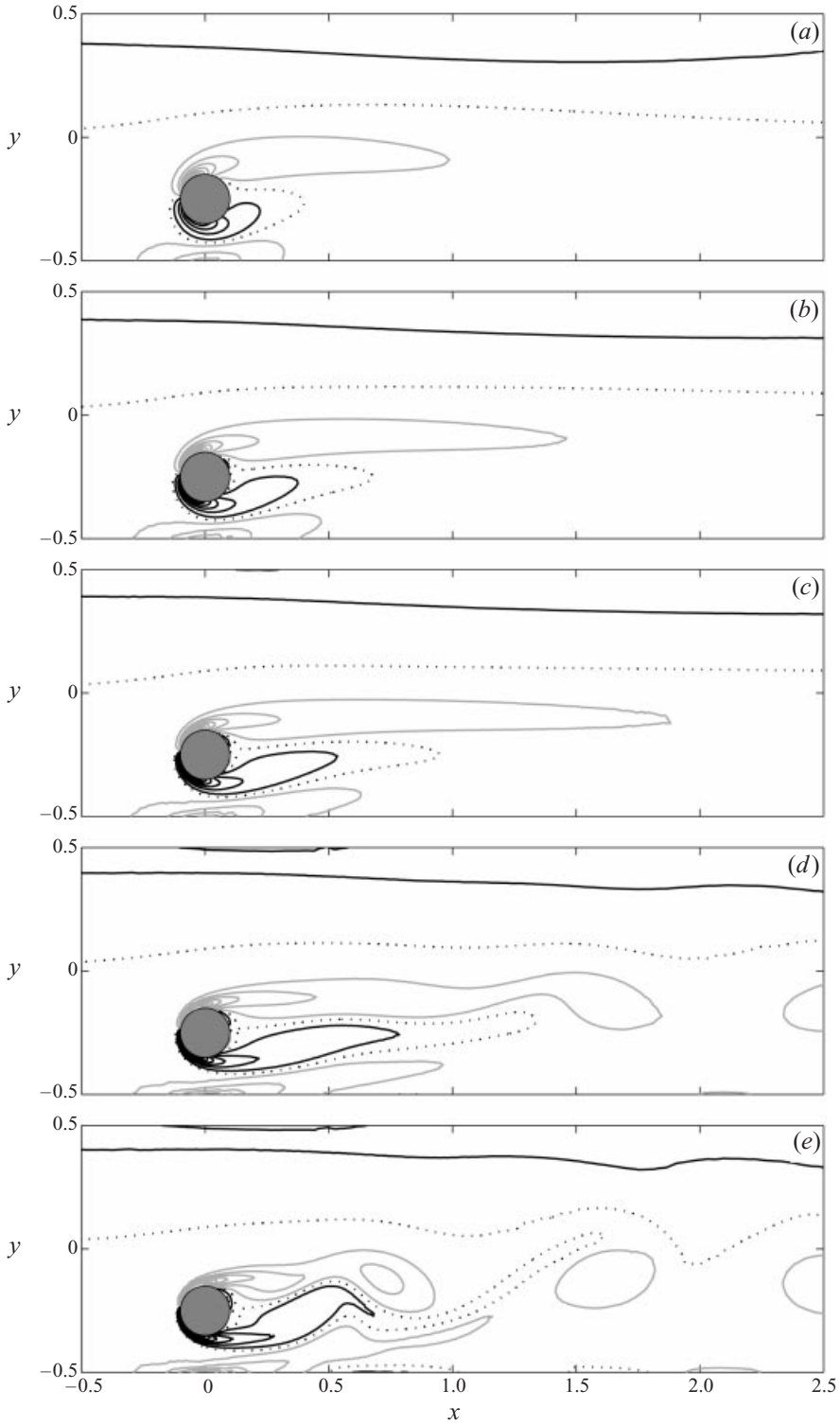


FIGURE 9. Flow vorticity contours for $\gamma = 0.75$ and (*a*) $Re = 100$, (*b*) 200, (*c*) 300, (*d*) 500, (*e*) 700: (*a*, *b*, *c*) are steady fields, (*d*, *e*) are instantaneous fields during the periodic regime.

https://doi.org/10.1017/S0022112001004608 Published online by Cambridge University Press

$\gamma \rightarrow$	2.00	1.75	1.25	0.75	0.25
$Re \downarrow$					
100	∞	∞	∞	∞	∞
200	∞	∞	∞	∞	∞
230	∞	∞			
240	0.85	∞			
250		0.85			
270	0.84	0.83	∞	∞	∞
275	0.84	0.83	∞	∞	∞
280	0.83	0.83	∞	∞	∞
290		0.82	∞		
300	0.81	0.81	0.84	∞	∞
400				∞	
450				∞	
500	0.73	0.74	0.76	(0.86)	∞
530				0.85	
600				0.84	
700				0.82	
1000	0.67	0.68	0.71	0.78	∞
1250					∞
1500					∞
1800					0.90
2000					0.90

TABLE 1. Dimensionless period T for different values of the Reynolds number Re and gap parameter γ.

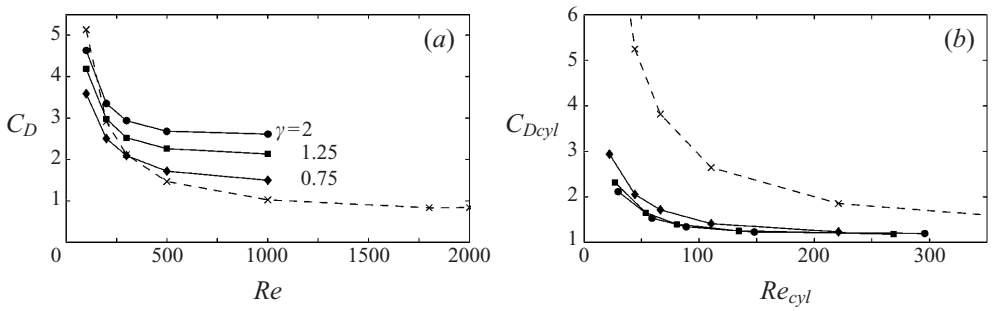


FIGURE 10. Mean drag coefficient dependence on the Reynolds number for $\gamma = 2$, 1.25, 0.75, 0.25: (*a*) standard quantities, (*b*) cylinder-based quantities. Symbols correspond to the same value of γ in both graphs.

et al. 1999), which can rotate, because of the lack of symmetry, or deform, because of the direct interaction with the wall. Consequently the drag and lift forces depend on the distance from the wall in addition to the Reynolds number.

The drag coefficient $C_D = \overline{F}_x/0.5d$, where $\overline{F}_x$ is the steady or time-average (for periodic flow) longitudinal component of the dimensionless force (i.e. dimensional force per unit length divided by $\rho U^2 H$), is plotted in figure 10(*a*) as a function of the Reynolds number for various values of the gap parameter. The drag coefficient has the expected decaying behaviour, for all gap values, with increasing Reynolds number. The shape is similar for gaps from 2 down to 0.75, even though the C_D value is reduced; the extreme case, $\gamma = 0.25$, has a higher C_D at low Reynolds numbers and a smaller one at large values. The reduction in the drag coefficient on approaching one wall was

https://doi.org/10.1017/S0022112001004608 Published online by Cambridge University Press

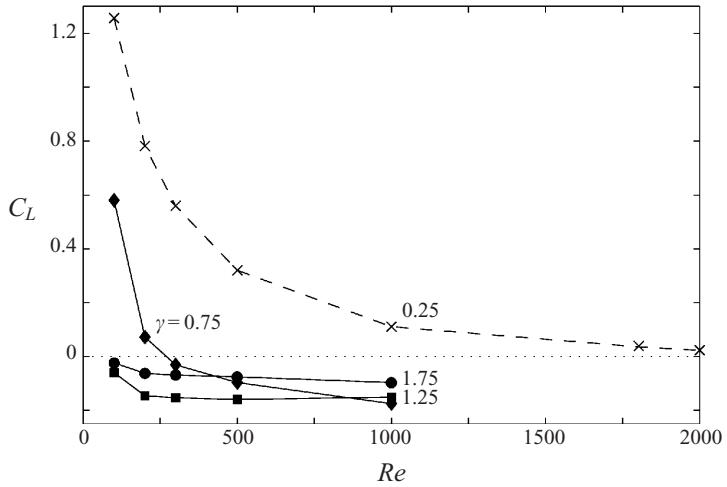


FIGURE 11. Mean lift coefficient dependence on the Reynolds number for $\gamma = 1.75, 1.25, 0.75, 0.25$.

previously observed at larger Reynolds number (Taniguchi & Miyakoshi 1990; Lei *et al.* 1999) as soon as the body penetrates the wall boundary layer. A more appropriate comparison among the results at different distances from the wall can be obtained by analysing the behaviour of a cylinder-based drag coefficient $C_{Dcyl} = C_D/v_{cyl}^2$ as it depends on the cylinder-based Reynolds number. This is illustrated in figure 10(*b*): the values obtained at gap values larger that 1 are in general agreement with the unbounded case, and slightly larger for $\gamma = 0.75$. The value of C_{Dcyl} is significantly larger when the cylinder is much closer to the wall. In such case the small gap is almost entirely occupied by the viscous boundary layers created on the lower side of the cylinder and on the facing wall (see figure 3*e*), the flow encounters a great resistance in passing through the viscous gap and is almost entirely turned above the body. As a consequence the body plus gap system behaves like a larger surface-mounted object.

The wall exerts a strong influence on the lift force. The lift coefficient $C_L = \overline{F}_y/0.5d$ is shown in figure 11 as a function of the Reynolds number for various values of the gap parameter. The lift takes positive or negative values depending on the values of the parameters. The graph suggests the existence of at least two different concurrent phenomena that produce positive and negative lift, respectively.

It is reported in the literature that the presence of a wall generally produces a repulsive force from it. This is found to be attributable to the confinement effect of the presence of the plane wall and, secondly, to the influence of the vorticity separated from it. A repulsive force has been found to act between a pair of cylinders side by side (Bearman & Wadcock 1973). In such a simple model the wall can be seen as an axis of symmetry between a pair of cylinders and therefore it only produces a confinement effect. When the cylinders approach each other the dividing streamline, which was in front of the cylinder in an unbounded flow, or at $\gamma = 2$, moves towards the wall; oppositely the wake on the rear of the body is confined on the wall side and is therefore deflected away from the wall. The eventual picture, as the cylinder approaches the wall, is a flow which is aligned in a direction slightly inclined, closer to the wall in front of the body and farther from it to the rear which produces a positive lift. This argument, which is based on an irrotational type of distortion of the flow, is essentially the same as developed by Kim, Elghobashi & Sirignano (1993)

https://doi.org/10.1017/S0022112001004608 Published online by Cambridge University Press

to explain the repulsion between two spheres placed symmetrically in a uniform flow. This positive lift is enhanced in presence of a real, no-slip, wall where the wall boundary layer may undergo a wake-induced separation. In such a case the separated vorticity interacts with the facing wake, and dissipate part of the closer wake vorticity. This additional, purely rotational, influence of the wall reduces the intensity of the body wake on the wall side and thus the resulting wake is stronger farther from the wall and enhances the repulsive, positive, lift.

In order to verify this picture, and also explain the observed negative lift, we analyse the flow about the body and the corresponding pressure distribution on the cylinder surface. Streamlines, at $Re = 200$, are shown in figure 12(*a–e*) for $\gamma = 2$, 1.75, 1.25, 0.75, 0.25, respectively; the corresponding pressure distributions are given in figure 12(*f–j*). The first Fourier azimuthal harmonics of the wall pressure are shown with radial lines because all other harmonics give null contribution to the forces on the body; nevertheless the actual pressure (with zero arbitrary mean) is also plotted in the same graph.

The streamlines show in all cases a deflection which is essentially the irrotational mechanism applied to the body plus wake system. As the body approaches the wall its wake decreases on the wall side and increases on the opposite side creating an unbalance in the rear pressure (negative, i.e. creating a specific force directed away from the body) and a net repulsive lift. This dynamics is evident for $\gamma = 0.25$, see figure 12(*e*, *j*), where a wall-side wake attached to the body is almost absent; this case corresponds to a large positive lift (see figure 11 for the actual values) and the associated pressure distribution points upward. At larger gaps the deflection is reduced and the wake is increasingly balanced. Nevertheless even though a small positive lift is present for $\gamma = 0.75$, corresponding to figure 12(*d*, *i*), a negative lift is found for $\gamma = 1.25$ and $\gamma = 1.75$, corresponding to figures 12(*c*, *h*) and 12(*b*, *g*), respectively. In these latter cases the distribution of pressure on the rear of the body is indeed almost balanced whereas a negative lift is caused by the distribution of pressure in front of the body. Pressure is higher on the side opposite to the wall simply because incoming velocity is higher there.

A mechanism leading to a negative contribution to the lift can be found in the presence of shear in the incoming velocity profile. Let us consider a velocity profile $v_x(y)$ in front of a cylinder placed at a position y_0. The longitudinal force, at a given Reynolds number, is of the form

$$F_x \sim d v_x^2(y_0). \tag{8}$$

We imagine dividing the cylinder in two halves above and below a line parallel to the walls. If we only consider the effect of the shear, thus ignoring the influence of the confining walls, the module of the force on the upper and lower halves can be estimated in the following form:

$$F^{(\pm)} \sim d \left(v_x(y_0) \pm \frac{d}{2} \left. \frac{\partial v_x}{\partial y} \right|_{y_0} \right)^2. \tag{9}$$

The lift can be obtained (because of symmetry between the two faces) as the difference between the lower and the upper forces (times a geometric coefficient), to eventually give

$$F_y \sim -d v_x(y_0) \left. \frac{\partial v_x}{\partial y} \right|_{y_0}, \tag{10}$$

https://doi.org/10.1017/S0022112001004608 Published online by Cambridge University Press

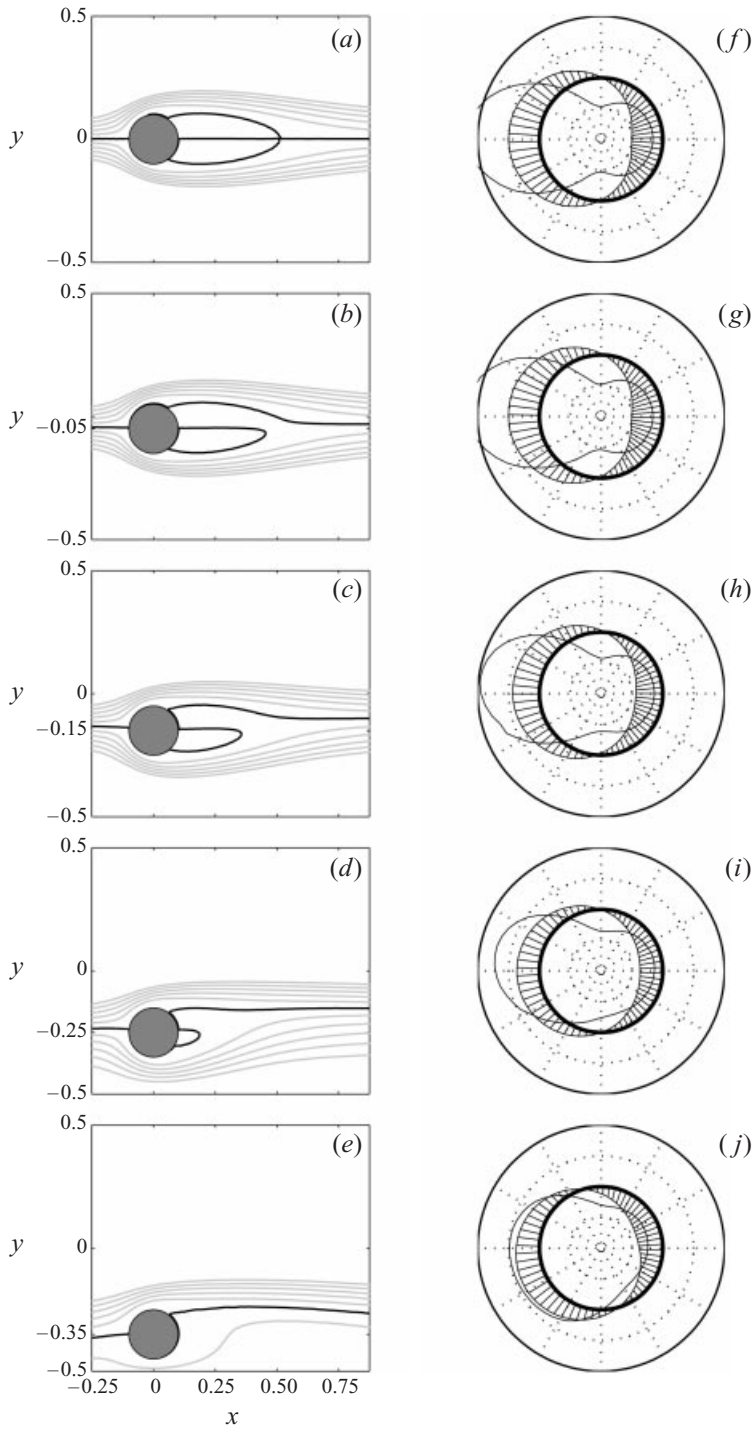


FIGURE 12. Steady flow at $Re = 200$ and (a, f) $\gamma = 2$, (b, g) $\gamma = 1.75$, (c, h) $\gamma = 1.25$, (d, i) $\gamma = 0.75$, (e, j) $\gamma = 0.25$. $(a$–$e)$ Streamlines, streamfunction levels from the dividing streamline (black) with increments ± 0.02. $(f$–$j)$ Pressure on the cylinder, first azimuthal harmonic (with lines connected to the zero level) and complete signal with zero mean. Radial pressure levels are -300 (centre), -150, 0 (thick circle), 150, 300 (outer circle).

https://doi.org/10.1017/S0022112001004608 Published online by Cambridge University Press

which gives a negative lift as a consequence of a positive shear. If we define a shear number

$$\sigma = \frac{d}{v_x(y_0)} \left. \frac{\partial v_x}{\partial y} \right|_{y_0}, \tag{11}$$

we obtain the following approximate linear relationship:

$$\frac{F_y}{F_x} \sim -\sigma, \tag{12}$$

where the proportionality coefficient is of order one and should not be, or is only weakly, dependent on the Reynolds number.

The influence of shear on the lift has been widely investigated in the case of a spherical body close to a wall, because of its relevance for the settling velocity of solid particles and for dispersion of droplets. The fundamental work by Saffman (1965) shows a square-root dependence of lift on shear in the case of moving particles. The more recent work by Cherukat & McLaughlin (1993, see appendix by P. M. Lovalenti) shows the presence of a negative linear contribution to the lift force, similar to (10), on a small sphere translating in a shear near a wall. However, these results are obtained in the limit of particle-based Reynolds number much smaller than 1, when forces are essentially of viscous type. The argument presented above, and leading to the scaling (12), is essentially based on pressure forces, i.e. with a quadratic velocity scaling.

To check relation (12) without the possible influence of other effects we have performed three simulations with the cylinder placed in the centre of the channel ($\gamma = 2$) and the walls moving at different velocities to produce a constant shear velocity profile. The Reynolds number is fixed at $Re = 200$ (to have steady flows), which corresponds to $Re_{cyl} = 40$, and shear number $\sigma = 0.1, 0.2, 0.4$. The relation between the forces ratio and σ is reported with open circles in figure 13 where the good approximation given by a linear relation (12) is evident.

On the same picture the values obtained in the normal simulations at various distances from one wall and Reynolds numbers are shown. It must be kept in mind that, given the upstream parabolic profile, there is a correspondence between the parameter γ and the shear number (indicated with the arrows pointing to the σ-axis). The forces are a result of the shear-induced negative lift and of the positive lift given by the presence of the near wall as discussed above.

The repulsion effect due to the wall is of little significance for large gap sizes: its strength also decreases with growing Reynolds number. This is seen in figure 13 where the results approach the asymptotic behaviour (12) indicated by the open circles, at large γ and at growing Reynolds number. At smaller distances from one wall the dominance of repulsion is observable, and as explained above it is more marked at smaller Reynolds number. It must be pointed out that the cylinder-based Reynolds number decreases for smaller gap sizes (see equations (6), (7)), which enhances the dominance of positive lift close to the wall. In conclusion we can affirm that, even though repulsion is the most common phenomenon (Bearman & Wadcock 1973; Bearman & Zdravkovich 1978), the presence of shear explains the possible appearance of the negative lift as observed in figure 11.

A negative lift is found in the case of a plane turbulent boundary layer (Lei *et al.* 1999), particularly noticeable in the case of a higher shear boundary layer. A significant agreement is found with the results in the presence of shear without walls (Nakabayashi *et al.* 1993). These data (see their table 1), also reported in figure 13, show negative lift with an evident linear relation with the shear confirming relation

https://doi.org/10.1017/S0022112001004608 Published online by Cambridge University Press

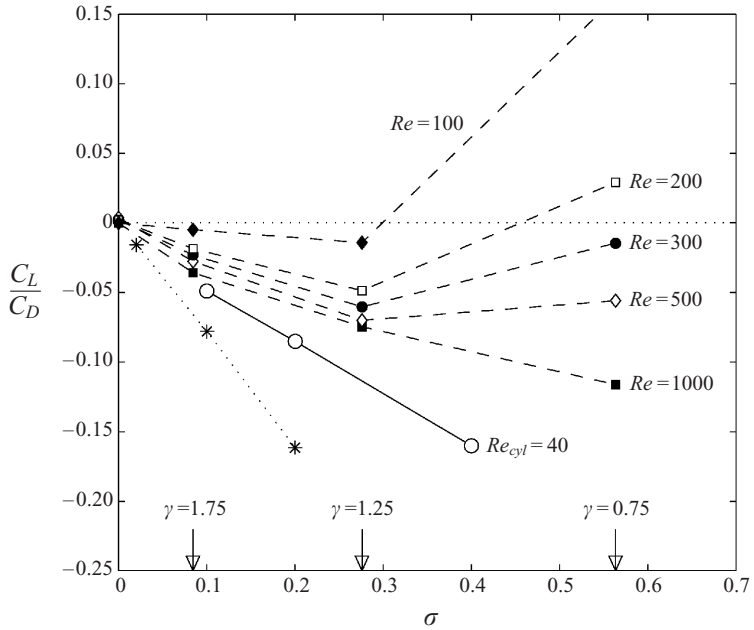


FIGURE 13. Ratio of the mean lift and drag coefficients as a function of the shear number. The symbols with dashed lines correspond to various Reynolds numbers (as indicated on each curve) and gap parameter (the values $\gamma = 2$, 1.75, 1.25, 0.75 in a parabolic profile correspond to $\sigma = 0$, 0.084, 0.276, 0.563, respectively). The open circles relate to the special case of a cylinder centred in a channel with constant shear velocity profile; the stars are from (Nakabayashi *et al.* 1993).

(12); the few observations of positive lift values reported there are found at high, order-one, shear values and are associated with strongly varying either drag or lift coefficients indicating, if confirmed, the presence of complex flow dynamics which cannot be taken into account in the simple reasoning leading to (12).

A weak attraction has been observed between two symmetric spheres in a uniform flow (Kim *et al.* 1993). We argue that this small effect may be caused by a small shear created by the pair of spheres themselves. Despite the geometric differences those results are in qualitative agreement with the present ones: repulsion is the dominant feature when the bodies are close each other, and a weak attraction appears in an intermediate range when these are further apart; furthermore the attraction is also slightly more pronounced at larger Reynolds number.

The trajectory of the unsteady force vector is reported in figure 14 for $\gamma = 0.75, 1.25, 2$ at $Re = 1000$, and $\gamma = 0.25$ at $Re = 2000$. The double loop at larger gap sizes is a consequence of the symmetric alternate shedding, in which the lift has twice the period of the drag. The lower loop decreases with respect to the larger one as the separation from the lower side of the body also reduces. This disappears for smaller gaps when shedding produces a single row of vortices.

6. Conclusions

The flow about a circular cylinder placed inside a plane channel, at various distances from the walls, has been studied numerically for values of the Reynolds number from those corresponding to steady flows and the initiation of the vortex shedding regime, to before the physical appearance of three-dimensional instabilities. The absence of

https://doi.org/10.1017/S0022112001004608 Published online by Cambridge University Press

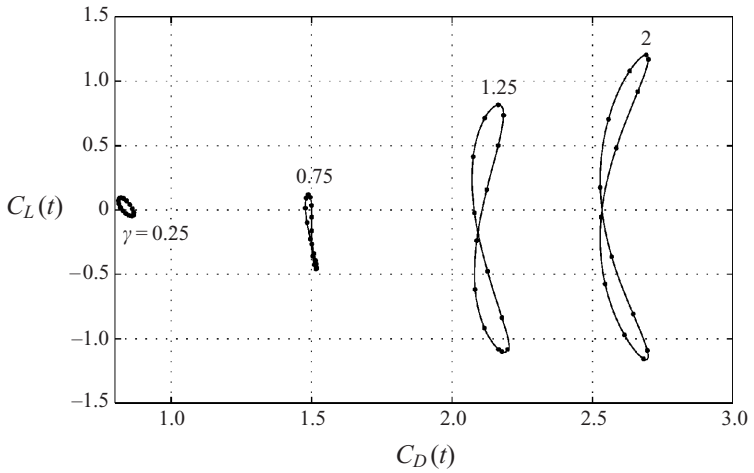


FIGURE 14. Trajectories in the lift and drag coefficients plane during a period in the periodic regime. For $\gamma = 2$, 1.25, 0.75 at $Re = 1000$, and $\gamma = 0.25$ at $Re = 2000$.

three-dimensional disturbances is inferred from the stability of both the channel flow and the unbounded flow about a cylinder at the values of the Reynolds number investigated here, with the exception of the highest Re, $\gamma = 0.25$, cases. The uncertainty for this specific case means that three-dimensional instabilities may or not be delayed by the presence of the walls compared to the case of a cylinder in unbounded flow. However the results show that the two-dimensional transition from steady to unsteady flow is significantly delayed by the presence of a close wall. Afterwards, in the unsteady regime, the presence of a wall inhibits the creation of a vortex pair and the wake becomes a single row of vortex filaments whereas the transition from two-dimensional to three-dimensional flow in the wake of an unbounded cylinder is caused by the self-induced stretching of the vortex pairs (Williamson 1996*b*).

A finite element numerical method has been employed, based on the vorticity–stream-function formulation, to exactly satisfy the conservation of mass with a divergence-free velocity field. The accuracy of the solutions has been checked.

It has been found that the transition from steady flow to a periodic vortex shedding regime occurs at larger Reynolds number as the cylinder approaches one wall, because the wake interacts with the wall boundary layer. The periodic shedding is delayed because the vorticity shed from the cylinder's wall side couples with the wall vorticity which arrests its evolution. Eventually the close proximity of one wall can inhibit the appearance of vortex shedding. It is shown that when the distance from the wall is smaller than half the cylinder radius the vortex shedding regime only occurs at such large values of the channel Reynolds number that the flow may have already undergone a transition to three-dimensional flow.

In the unsteady regimes, when the body is far enough from one wall, the vortex shedding pattern is similar to the von Kármán vortex street, even if the confinement due to the channel walls produces an inversion on the position of vortices. When the cylinder is closer to one wall the two layers of opposite sign vorticity, separated from the cylinder and from the wall, form a pair of vortex sheets which dissipate during the mutually induced stretching. As a result, for distances smaller than the cylinder diameter (at sufficiently high Re to have an unsteady regime), the von Kármán street is substituted by a unique row of like-signed vortices.

https://doi.org/10.1017/S0022112001004608 Published online by Cambridge University Press

For all wall–cylinder distances greater than about one cylinder diameter, the variation of the mean drag coefficient with the Reynolds number, once these are normalized with the local velocity in front of the body, is essentially the same, despite the phenomenological differences in the flow. This is not true when the cylinder is very close to the wall when the body behaves like a larger surface-mounted obstacle with a larger resistance.

The lift force is shown to be composed, in a first approximation, of two different contributions: a repulsive and an attractive one. The repulsive component, previously observed by other authors, is caused by the deflection of the wake away from the body due to the wall confinement, an effect which is enhanced by the separation of the wall boundary layer whose vorticity interacts with and dissipates part of the wake vorticity which is closer to the wall. As a result the body wake, and the corresponding low pressure zone, is stronger on the side farther from the wall and pulls the body away from it. An attractive lift has also been observed in some cases. It has been shown that the negative lift is a consequence of the shear in front of the body. The velocity profile gives a higher pressure on the face farther from the wall than on the lower one resulting in a force towards the wall. An estimate for this has been given.

The authors wish to thank Dr F. Domenichini for several discussions during the development of this work and Dr V. Armenio for suggesting pertinent references. The authors acknowledge financial support from the Italian MURST "ACME-CUE" project.

REFERENCES

Batchelor, G. K. 1967 *An Introduction to Fluid Dynamics*. Cambridge University Press.

Bearman, P. W. & Wadcock, A. J. 1973 The interaction between a pair of circular cylinders normal to a stream. *J. Fluid Mech.* **61**, 495–511.

Bearman, P. W. & Zdravkovich, M. M. 1978 Flow around a circular cylinder near a plane boundary. *J. Fluid Mech.* **89**, 33–47.

Chen, J.-H., Pritchard, W. G. & Tavener, S. J. 1995 Bifurcation for flow past a cylinder between parallel planes. *J. Fluid Mech.* **284**, 23–41.

Cherukat, P. & Mclaughlin, J. B. 1994 The inertial lift on a rigid sphere in a linear shear flow field near a flat wall. *J. Fluid Mech.* **263**, 1–18.

Dütsch, H., Durst F., Becker, S. & Lienhart, H. 1998 Low-Reynolds-number flow around an oscillating circular cylinder at low Keulegan-Carpenter numbers. *J. Fluid Mech.* **360**, 249–271.

Grass, A. J., Raven, P. W. J., Stuart, R. J. & Bray, J. A. 1984 The influence of boundary layer velocity gradient and bed proximity on vortex shedding from free spanning pipelines. *ASME J. Energy Resour. Tech.* **106**, 70–78.

Justensen, P. 1991 A numerical study of oscillating flow around a circular cylinder. *J. Fluid Mech.* **222**, 157–196.

Karniadakis, G. E., Mikic, B. B. & Patera, A. T. 1988 Minimum-dissipation transport enhancement by flow destabilization: Reynolds' analogy revisited. *J. Fluid Mech.* **192**, 365–391.

Kim, I., Elghobashi, S. & Sirignano, W. A. 1993 Three-dimensional flow over two spheres placed side by side. *J. Fluid Mech.* **246**, 465–488.

Lei, C., Cheng, L. & Kavanagh, K. 1999 Re-examination of the effects of a plane boundary on force and vortex shedding of a circular cylinder. *J. Wind Eng. Ind. Aer.* **80**, 263–286.

Nakabayashi, K., Yoshida, N. & Aoi, T. 1993 Numerical analysis for viscous shear flows past a circular cylinder at intermediate Reynolds number. *JSME Intl J.* B **36**, 34–41.

Pedrizzetti, G. 1996 Unsteady tube flow over an expansion. *J. Fluid Mech.* **31**, 89–111.

Saffman, P. G. 1965 The lift on a small sphere in a slow shear flow. *J. Fluid Mech.* **22**, 385–400.

Saiac, J. H., Santi, F. & Mai, V. P. 1995 Numerical solution of the Navier–Stokes equations by a Lagrange-Galerkin method coupling u, p and ψ, ω formulations. In *Proc. IX Intl Conf. on Finite Elements in Fluids, New Trends and Applications, IACM-Special Interest Conference* (ed.

https://doi.org/10.1017/S0022112001004608 Published online by Cambridge University Press

M. Morandi Cecchi, K. Morgan, J. Periaux, B. A. Schrefler & O. C. Zienkiewicz), Part 1, pp. 285–295. S. M. Legatozia, Padova.

Sohankar, A., Norberg, C. & Davidson, L. 1999 Simulation of three-dimensional flow around a square cylinder at moderate Reynolds number. *Phys. Fluids* **11**, 288–306.

Sumer, B. M., Jensen, B. L. & Fredsoe, J. 1991 Effect of a plane boundary on oscillatory flow around a circular cylinder. *J. Fluid Mech.* **225**, 271–300.

Taniguchi, S. & Miyakoshi, K. 1990 Fluctuating fluid forces acting on a circular cylinder and interference with a plane wall. *Exps. Fluids* **9**, 197–204.

Tatsuno, M. & Bearman, P. W. 1990 A visual study of the flow around an oscillating circular cylinder at low Keulegan–Carpenter numbers and low Stokes numbers. *J. Fluid Mech.* **211**, 157–182.

Williamson, C. H. K. 1996*a* Vortex dynamics in the cylinder wake. *Ann. Rev. Fluid Mech.* **28**, 477–539.

Williamson, C. H. K. 1996*b* Three-dimensional wake transition. *J. Fluid Mech.* **328**, 345–407.

Zienkiewicz, O. C. 1977 *The Finite Elements Method*, 3rd Edn. McGraw-Hill.

https://doi.org/10.1017/S0022112001004608 Published online by Cambridge University Press